Boosting the Performance of Ionic-Liquid-Based Supercapacitors with Polar Additives

Journal:	*The Journal of Physical Chemistry*
Manuscript ID	Draft
Manuscript Type:	Article
Date Submitted by the Author:	n/a
Complete List of Authors:	Liu, Kun; University of California at Riverside, Department of Chemical and Environmental Engineering Wu, Jianzhong; University of California at Riverside, Department of Chemical and Environmental Engineering

Boosting the Performance of Ionic-Liquid-Based Supercapacitors with Polar Additives

Kun Liu and Jianzhong Wu*

Department of Chemical and Environmental Engineering, University of California, Riverside, CA 92521, USA

ABSTRACT

Recent years have witnessed growing interests in both the fundamentals and applications of electric double layer capacitors (EDLCs), also known as supercapacitors. A number of strategies have been explored to optimize the device performance in terms of both the energy and power densities. Because the properties of electric double layers (EDL) are sensitive to ion distributions in the close vicinity of the electrode surfaces, the supercapacitor performance is sensitive to both the electrode pore structure and the electrolyte composition. In this work, we study the effects of polar additives on EDLC capacitance using the classical density functional theory within the framework of a coarse-grained model for the microscopic structure of the porous electrodes and room-temperature ionic liquids. The theoretical results indicate that a highly polar, low-molecular-weight additive is able to drastically increase the EDLC capacitance at low bulk concentration. Additionally, the additive is able to dampen the oscillatory dependence of the capacitance on the pore size thereby boosting the performance of amorphous electrode materials. The theoretical predictions are directly testable with experiments and provide new insights into the additive effects on EDL properties.

* Corresponding Author. E-mail: jwu@engr.ucr.edu

TOC GRAPHICS

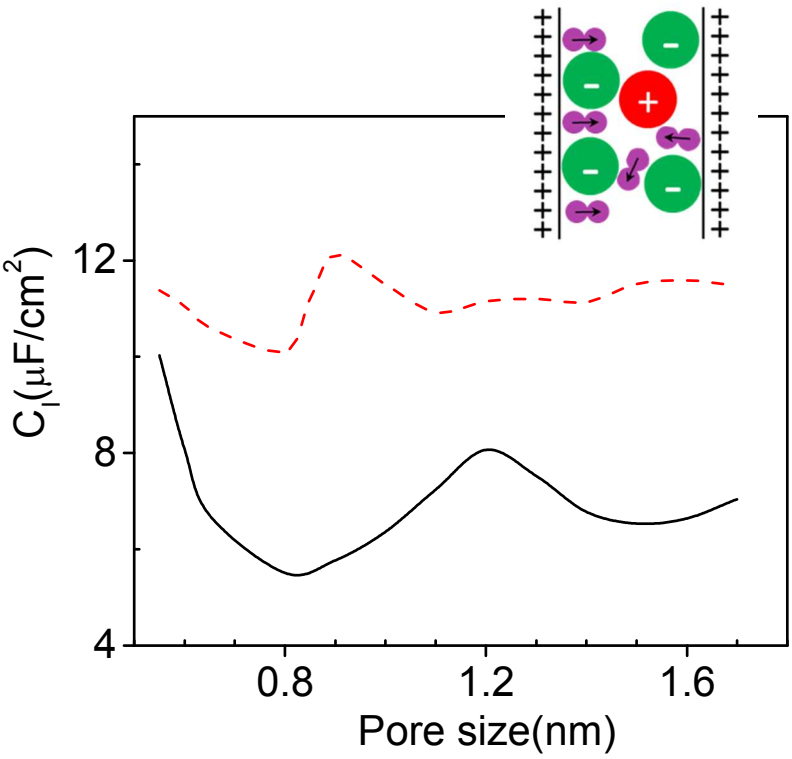

KEYWORDS: Electric double layer (EDL), Energy storage, Classical density functional theory

I. Introduction

Electric double layer capacitors (EDLCs), also called supercapacitors or ultracapacitors, have the advantages of high power density and long cycle life in comparison to alternative energy storage devices. In supercapacitors, the electrical energy is stored by revisable adsorption of ionic species onto the surface of typically porous electrodes, leading to the formation of an electric double layer (EDL) – layering of opposite charge at the electrolyte-electrode interface.[1] A major effort for the ongoing research on supercapacitors is to address the limitation of their moderate energy density.[2,3] One of the key strategies is to identify electrolyte-electrode pairs that can optimize the equilibrium and transport properties of the charge carriers.[4-7] Because the EDLC performance is directly related to preferential adsorption of cations or anions into the micropores of the electrodes, an appropriate combination of the electrode material and the working electrolyte plays a pivotal role for the rational design and optimization of supercapacitors.[8-11]

Whereas a wide variety of porous materials, with tuned pore size distributions, morphology, architecture and functionality, has been proposed as the supercapacitor electrodes,[12,13] most porous electrodes in practical use are made of carbon materials such as activated carbon, templated carbons, carbon aerogels, carbide-derived carbons, carbon nanotubes and graphenes.[14] Porous carbons are attractive owing to relatively low cost, easy processing, non-toxicity, high chemical stability, large electrical conductivity, and large specific surface area. Meanwhile, diverse electrolytes have been tested to enhance the EDLC performance.[15] Although existing supercapacitors are mostly based on conventional electrolytes such as aqueous or organic solutions of small ions, room-temperature ionic liquids (ILs) are promising for future applications because they enable electric charging at a much higher voltage, thus greatly increase

the energy density.[16] Besides, ILs have the advantages of low vapor pressure and non-flammability, allowing them to be used safely over a wide temperature range.[17,18]

Although porous carbons with a broad spectrum of pore sizes and shapes have been investigated as the electrodes, previous studies are mostly focused on pure ionic liquids, i.e., electrolytes consisting of one type of cation and one type of anion. The effect of electrolyte composition and electrode structure on the EDLC performance is not completely understood.[19] For example, a number of experimental and theoretical reports indicate that the surface-area-normalized capacitance may be drastically increased as the pore size becomes comparable to the dimensionality of the ionic species.[20-26] But complications often arise from the experimental side in terms of how the values of the surface area and the pore size distribution are determined and how the effects of the pore size dispersity are taken into account for realistic electrodes.[27] While both theory and molecular simulations predict an oscillatory dependence of the capacitance on the electrode pore size[28-30], direct validation of the theoretical results with experimental measurements is difficult due to the lack of a precise control of the electrode pore size. Contradictory results have also been reported on the effects of electrolyte composition on the EDL structure and capacitance. Based on molecular dynamics (MD) simulations, Feng et al. found that the EDL capacitance increases only slightly for 1-butyl-3-methylimidazolium tetrafluoroborate ([BMIM][BF_4]) near either a positive or a negative electrode when it is diluted with acetonitrile (ACN) up to 50% in the mass fraction.[31] However, simulation results by Shim et al. indicate that the capacitance of 1-ethyl-3-methylimidazolium tetrafluoroborate ([EMIM][BF_4]), a similar ionic liquid, is higher than that in a binary mixture of IL and acetonitrile by 55–60%.[32] Recent experiment and theoretical studies show that solvent addition

to an IL may lead to a significant increase of the capacitance and that an optimum composition can be identified to maximize the EDLC performance.[33,34]

Built upon our previous studies of the structure and capacitance of electrolyte/electrode interfaces[28], we investigate in this work the effects of polar additives on IL-based EDLCs by using the classical density functional theory (CDFT). While the solvent effects were studied in our previous publications[26,35], the additives interact with the electrode surface and ionic species in unique ways such that they may have drastic effects on supercapacitor performance even at very low concentration. To our knowledge, the special additive effects have not been investigated before but could open up a new direct of research for design and optimization of EDLCs. We demonstrate that the oscillatory dependence of the capacitance on the pore size can be strongly alleviated by the use of a polar additive, in addition to an overall increase of the capacitance. The theoretical results open up new perspectives on additive effects and may usher in new experimental studies on the use of low-concentration additives.

II. Molecular model and methods

We consider the additive effects on the performance of electric double layer (EDL) capacitors consisting of porous carbons and room-temperature ionic liquids. Because the carbon material has a dielectric constant not much different from that of a typical ionic liquid (~10-20), the polarizability effect or "electronic screening" is relatively insignificant for such systems. Like our previous studies[26,28,30,35], we use a slit-pore model for the porous electrode, which is fully consistent with that typically used for the characterization of amorphous porous materials in experiments. For simplicity, the restricted primitive model is used to represent cations and anions in an ionic liquid. The cations and anions have the same diameter ($\sigma_i = 0.5\,\text{nm}$) but opposite valence ($Z_i = \pm 1$). Approximately, the model parameters match those corresponding to

1-ethyl-3-methylimidazolium bis(trifluoromethyl- sulfonyl) imide (EMIM-TFSI), an ionic liquid commonly used in electrochemical devices. At 298 K and 1 bar, the molar volume of EMIM-TFSI is 259 cm^3/mol, corresponding to a reduced number density of $\rho_i \sigma_i^3 = 0.29$ for both cations and anions[30].

The additive molecules are represented by two tangentially connected spheres of the same size but opposite charges. While the simple model does not reveal atomic details as provided by realistic force fields used in molecular dynamics simulations, it captures the essential features important for understanding the charging behavior of ionic liquids. In particular, it accounts for electrostatic correlations and ionic excluded volume effects important for understanding the supercapacitor performance but neglected in conventional electric double layer (EDL) theories. Similar models have been extensively used to study a broad range of parameters such as pore size, ion and solvent densities, ionic valences, surface energy and electric potential.

As in the primitive model for aqueous electrolyte solutions, the pair potential between charged spheres i and j is given by

$$\beta u_{ij}(r) = \begin{cases} \infty, & r < \sigma_{ij}/2 \\ Z_i Z_j l_B / r, & r \geq \sigma_{ij}/2 \end{cases} \quad (1)$$

where $\beta = 1/(k_B T)$ with k_B and T being the Boltzmann constant and the absolute temperature (fixed at 298 in this work), respectively, r is the center-to-center distance between particles i and j, and $\sigma_{ij} = (\sigma_i + \sigma_j)/2$. Parameter l_B is the Bjerrum length, which is equal to 556.9 Å, a value that corresponds to electrostatic interaction in vacuum at 298 K. We assume that dielectric constant is unity because the IL model accounts for pair interactions among all components explicitly.

The porous electrode is modeled as a slit pore with two symmetric hard walls. Inside the slit pore, the electrical field due to the surface charge density is uniform. As a result, each ionic species experiences a constant external potential in the direction perpendicular to the surface:

$$\beta V_i(z) = \begin{cases} -2\pi l_B Z_i HQ/e, & \sigma_i/2 \le z \le H-\sigma_i/2 \\ \infty, & \text{otherwise} \end{cases} \quad (2)$$

where z is the perpendicular distance of the center of the sphere from the surface, Q is the surface charge density (C/m^2), and H stands for the surface-to-surface separation(or pore width).

The theoretical details of the classical density functional theory (CDFT) have been reported in previous publications[26,35,36]. Here we recapitulate only the key equations and refer the readers to our earlier articles for the details. Intuitively, one may understand CDFT as a formal generalization of the Poisson-Boltzmann (PB) equation to account for ionic excluded volume effects and electrostatic correlations that are not negligible for ionic liquids. For given bulk densities of the ions and the additive molecules, temperature, the pore size, and the surface potential, we solve for the one-dimensional density profiles of cations and anions, $\rho_\alpha(z), \alpha = \pm 1$ as well as the additive segments, $\rho_\gamma(z)$, $\gamma = \delta\pm$, across the slit pore by minimizing the grand potential:[37,38]

$$\Omega = F\left[\rho_0(\mathbf{R}), \rho_\alpha(\mathbf{r})\right] + \int d\mathbf{R}\rho_0(\mathbf{R})[V_0(\mathbf{R}) - \mu_0] + \sum_{\alpha=+,-}\int d\mathbf{r}\rho_\alpha(\mathbf{r})\left[V_\alpha(\mathbf{r}) - \mu_\alpha\right] \quad (3)$$

where $\mathbf{R} \equiv (\mathbf{r}_{\delta+}, \mathbf{r}_{\delta-})$ are two coordinates specifying the positions of two additive segments, μ_α is the chemical potential of the ion α , μ_0 is the chemical potential of the additive, $V_\alpha(\mathbf{r})$ stands for the external potential of cations and ions, and $V_0(\mathbf{R})$ is the external potential for additive molecule, i.e. $V_0(\mathbf{R}) = V_{\delta+}(\mathbf{r}_{\delta+}) + V_{\delta-}(\mathbf{r}_{\delta-})$, and F is the intrinsic Helmholtz energy.

The number densities of the positive and negative segments $\rho_{\delta+}(\mathbf{r})$ and $\rho_{\delta-}(\mathbf{r})$ are calculated from

$$\rho_{\delta+}(\mathbf{r}) = \int d\mathbf{R}\delta(\mathbf{r}-\mathbf{r}_1)\rho_0(\mathbf{R}) \tag{4}$$

$$\rho_{\delta-}(\mathbf{r}) = \int d\mathbf{R}\delta(\mathbf{r}-\mathbf{r}_2)\rho_0(\mathbf{R}) \tag{5}$$

In Eq.(3), the intrinsic Helmholtz free energy F includes an ideal-gas contribution and excess

$$\beta F = \int d\mathbf{R}\rho_0(\mathbf{R})\left[\ln\rho_0(\mathbf{R})-1\right] + \beta\int d\mathbf{R}\rho_0(\mathbf{R})V_b(\mathbf{R}) + \sum_{\alpha=+,-}\int d\mathbf{r}\rho_\alpha(\mathbf{r})\left[\ln\rho_\alpha(\mathbf{r})-1\right] + \beta F^{ex} \tag{6}$$

where V_b stands for the bonding potential of the additive molecules

$$\exp[-\beta V_b(\mathbf{R})] = \frac{\delta(|\mathbf{r}_{\delta+}-\mathbf{r}_{\delta-}|-\sigma_{\delta\pm})}{4\pi\sigma_{\delta\pm}^2} \tag{7}$$

in which $\delta(r)$ is the Dirac function, $\sigma_{\delta\pm} = (\sigma_{\delta+}+\sigma_{\delta-})/2$ is the distance between the segments. F^{ex} is the excess Helmholtz free energy arising from the thermodynamic non-ideality (*viz.* due to the exclude-volume effect and electrostatic interactions). In this work, we use the modified fundamental measure theory to account for the hard-sphere repulsion, the first-order thermodynamic perturbation theory to account for the chain connectivity, and a quadratic functional expansion to account for the electrostatic correlations.[36,39-42] In previous publications [30,37], we have calibrated the theoretical performance of the course-grained model and the CDFT calculations with experimental results for both the capacitance and the ionic distributions.

III. Results and Discussion

To capture the generic features of the additive effects, we assume that a polar additive can be represented by two tangentially connected hard spheres that have the same diameter but opposite charges.[26,30,35] The dipole moment can be tuned by changing either the partial charge or the diameter for each segment (e.g., two hard-sphere segments that have a diameter of 0.2 nm

and an opposite charge of 0.208 e yield an electrical dipole moment of 2.0 D). To investigate the additive effects, we fix the mole fraction of the additive molecules in the bulk at a small value

$$x_0 = \frac{\rho_0}{\rho_0 + \rho_+ + \rho_-} = 10^{-4} \tag{8}$$

where ρ_0, ρ_+ and ρ_- are the number densities of polar additives, cations and anions in the bulk, respectively.

We began our analysis of the additive effect by examining its influence on the microstructure of EDLs in a single nanopore. Figure 1 presents the CDFT predictions for the local number densities of different species across a 1.2 nm slit pore**.** For all cases, the additive molecules are assumed to have the same segment diameter of 0.2 nm but with different dipole moments. When the electrode is grounded (*viz.*, 0 V at the surface), the distributions of the positive and negative particles are identical, as shown in Figure 1(a-d), due to the symmetry in the model parameters. While cations and anions are found to accumulate primarily near the electrode surface, the additive molecules form a multilayer structure owing to its smaller segment size. Despite its low bulk concentration, $x_0 = 10^{-4}$, a significant amount of additive molecules are accumulated inside the neutral pore, and the additive enrichment is enhanced when its dipole moment increases. Even without any direct attraction from the surface, the average ion density inside the pore is significantly larger than that in the bulk, and the dipole-ion correlations are mainly responsible for the enrichment of the additive molecules. From the density profiles, we can calculate the partition coefficient for the additive molecules, defined as its average concentration inside the pore divided by that in the bulk, and find that it increases from 2.67 to 675 when the additive dipole moment is raised from 2.0 to 3.5 Debye. The tremendous increase

in the partition coefficient indicates the importance of electrostatic correlations for the confined electrolyte.

Figure 1 (e-h) shows the EDL structure in the presence of a surface electrical potential (+1.5 V). In Fig 1(f-h), the peak positions between the density profiles of anions and the positive segment of the polar additive are less than 0.5 A apart because both types of particles are distributed close to the surface. Because the electric potential at the pore surface is fixed at +1.5 V, the additives have little effects on coion (cation) distributions. The surface charge leads to alternating layering of cations and anions in the slit pore, regardless of the dipole moment of the additives. The ion distributions, especially the density profile for anions (counterions in this case), are noticeably affected by the presence of additive molecules. One can see that the EDL consists of not only a layer of counterions but also a layer of additive molecules. The polar molecules accumulate mainly on the electrode surface and its adsorption inside the pore is strongly correlated with the dipole moment. The density profile for the positive segment of the additive molecules becomes much more localized as the dipole moment increases and followed by a strong layer of the negative segments, suggesting that the polar molecules are aligned perpendicular to the surface, in contrast to that near a neutral surface.

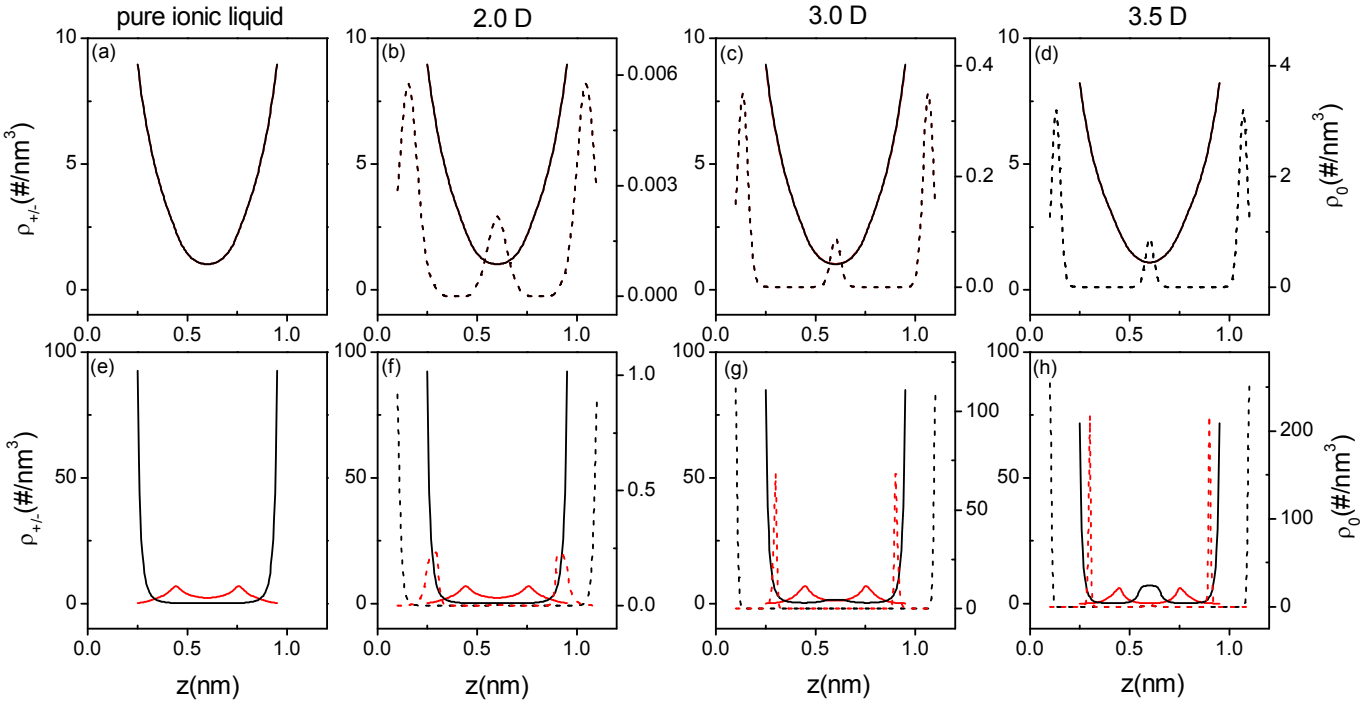

Figure 1. The number densities of anions (black solid lines) and cations (red solid lines), $\rho_{+/-}$, and the number densities of the negative (black dashed lines) and the positive segments (red dashed lines) of the additive molecules, ρ_0, across a 1.2 nm slit pore. Here the surface electrical potential is 0 V for panels (a-d) and +1.5 V for panels (e-h). In all cases, the mole fraction of the polar additive in the bulk is fixed at $x_0 = 10^{-4}$. The four columns correspond to a pure ionic liquid (3.8 M) and those with an additive of dipole moment of 2.0 D, 3.0 D and 3.5 D, respectively.

One important question about the additive effects is how they change the energy density for the charge storage or, more specifically, the surface charge and the EDL capacitance. The net electrical charge of the electrode includes several contributions: adsorption of counterions, swapping of coions for counterions, and desorption of coions from the porous electrode.[43,44] For a given electrode and an electrolyte pair, all these contributions depend on the electrode voltage. To identify these different contributions to the surface charge density, we present in Fig. 2 the influence of the electrode potential on the contact densities of counterions and the negative segments of the additive molecules. Here the contact number density of each species is defined as

$$\rho_{c,i} = \rho_i(z = \sigma_i / 2) \tag{9}$$

where σ_i is the diameter of particle i. The composition of the contact layer reflects a competition between the counterions and the additive molecules.

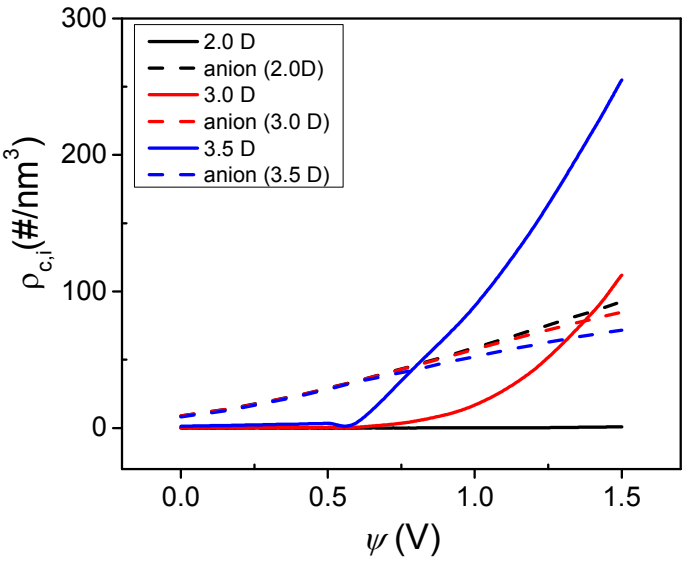

Figure 2 The contact densities of the anions (dashed lines) and the negative segment of the additive molecule (solid lines) *versus* the surface electrical potential. Here the pore width is fixed at 1.2 nm, the solid lines correspond to the additives with a dipole moment of 2.0 D, 3.0 D and 3.5 D, respectively.

At a low surface electrical potential, the additive effect on the adsorption of counterions is insignificant because its density in the contact layer is negligible compared to that of the counterions. When the surface electrical potential is beyond a threshold, however, the additive density in the contact layer dramatically increases with the electrical potential. Because the contact densities are defined in terms of the particle radii, the electric potential for the negative segment of the additive molecules is much larger than that for the counterions (anions). Besides, the electric potential at the contact position of the additive segments is not screened by ionic species due to the excluded-volume effects. As a result, the contact density for the negative

segment of the additive molecules increases more drastically with the surface electric potential in comparison to that for the counterions. For similar reasons, the polarity has little effect on the counterion density even though the contact density for the additive is sensitive to its dipole moment. Nevertheless, the contact density of the counterions is noticeably reduced due to the adsorptions of additive molecules. As shown in Fig. 1(h), their strong alignment at the surface leads to the formation of a counterion layer at the center of the slit pore, and the additional layer results an increase in the overall surface charge density. Figure 2 indicates that the additive effect is most significant under conditions of large dipole moment and high electrical potentials.

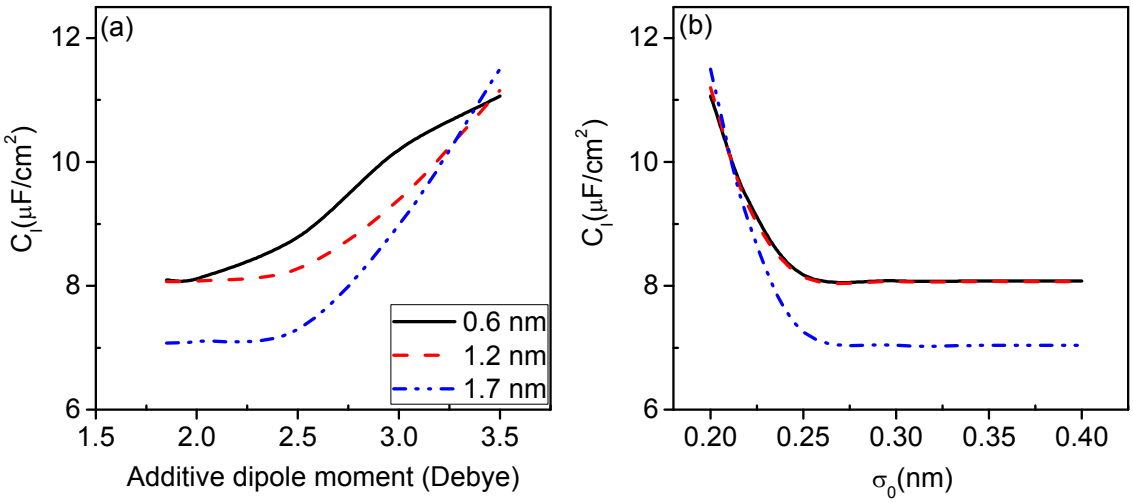

Figure 3 (a) Integral capacitance *versus* the dipole moment for additives of the same segment diameter ($\sigma_0 = 0.2$nm). Here the surface potential is fixed at +1.5 V, and different lines correspond to three representative pore widths. (b) The same as (a) but for additives of the same dipole moment of 3.5 D but different segment diameters (σ_0) in three pores.

To elucidate the effect of polar additives on the integral capacitance, we consider two key parameters in our coarse-grained model – dipole moment and segment size. Figure 3(a) shows the dependence of the integral capacitance versus the dipole moment while the segment diameter is fixed at σ_0 = 0.2 nm and the partial charge on each segment is treated as a variable. For three representative pores of different sizes, the integral capacitance increases as we raise the dipole

moment. In all three pores, a similar trend is observed on the effect of integral capacitance on the dipole moment. The increased capacitance can be attributed to stronger ion-dipole correlations and electrostatic attractions of additive molecules with the electrode. We find that adsorption of additives depletes more coions than counterions from the slit pore, leading to the drastic increase of the integral capacitance. The additives are mainly distributed at the pore center when the dipole moment is small but strongly accumulate at the electrode surface as the dipole moment increases (Fig 2). Such transition is clearly noticeable in a small pore as shown in Fig 3(a). As the pore size increases, the additive has little effects on the ionic distributions if the dipole moment is very small (see Fig 3a, H=1.7 nm). For additives with a strong polarity, however, their accumulation at the electrode surface results in a drastic increase of the capacitance because of the formation of multilayer structures concomitant to surface alignment. Interestingly, the capacitance appears independent of the pore size when the additives have a dipole moment of about 3.4 D. As discussed later, similar capacitances at these pores are resulted from the oscillatory dependence on the pore size.

Evidently, the additive size also plays an important role. If we fix the dipole moment of the additives as 3.5 D but vary the diameter of the additive molecules, the trend is quite different. As shown in Figure 3(b), the integral capacitance remains almost constant as the segment size increases beyond some threshold point (~ 0.25 nm). Beyond this segment size, the segment size has little effect on the integral capacitance. At a fixed dipole moment, the partial charge on each segment of the dimer will be reduced as the segment size increases thus the electrostatic attraction from the charged surface is reduced. While the increase in molecular volume hinders the additive entering the slit pore, the excluded volume effect becomes insignificant because of the low concentration of the additive molecules.

So far our calculations have been based on a single pore size, i.e., 1.2 nm slit pore. However, practical electrodes are mostly amorphous porous materials that do no have a precise control of the pore size distribution. One natural question is how the additive affects the pore size dependence of the capacitance.[45] To address this question, we present in Figure 4 the integral capacitance *versus* the slit pore width for the pure ionic liquid and its mixtures with additives of different dipole moments. It shows that the oscillatory dependence of the capacitance on the pore size is unaffected in the presence of a weakly polar additive at low concentration. In this case, the capacitance is hardly changed compared to that for the pure ionic liquid due to the negligible accumulation of additive molecules inside the pore. For additives with a larger dipole moment (3.0 D or 3.5 D), however, their accumulation inside the pore leads to a significant depletion of counterions (Fig. 2) from the contact layer and thus dampens the oscillatory dependence of the integral capacitance on the pore size. From Fig. 4, we see that two distinctive features stand out for highly polar additives: (a) the capacitance is drastically increased across the entire range of the pore size; and (b) capacitance oscillation in response to the changing pore size is greatly depressed.

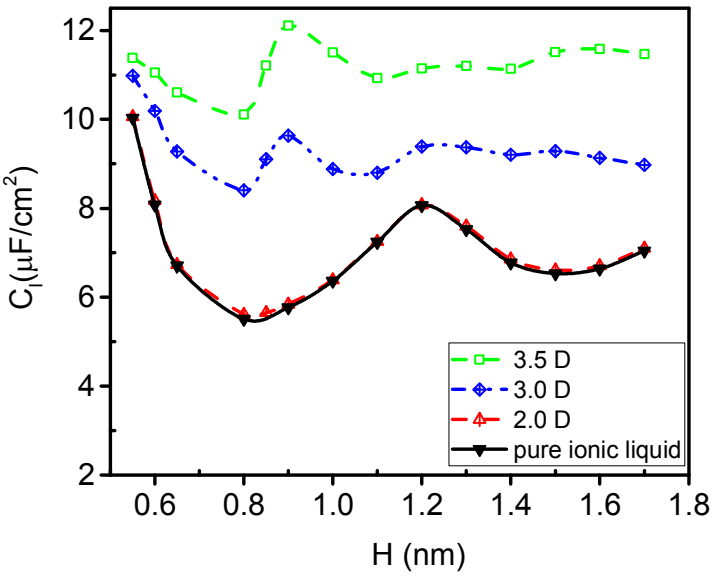

Figure 4 Integral capacitance *versus* the pore size for the pure ionic liquid and its mixture with additives of different dipole moments. Here the surface potential is fixed at +1.5 V and the segment diameter of the additive molecules is $\sigma_0 = 0.2\text{nm}$.

To further understand the additive effects on the integral capacitance, we analyze the density profiles of all chemical species in different pores. Figure 5 shows that, regardless of the pore size, addition of polar molecules leads to not only drastic changes in the EDL structure, as evidenced in their strong alignment near the surface, but also depletion of coions from the pore. Such effects become more pronounced as the dipole moment of the additive increases. The coion depletion explains the increase in the integral capacitance as shown in Figure 4. For a given additive (*viz*., the same dipole moment), the EDL structures are essentially the same as the pore size changes (such 0.9 nm and 1.5 nm), explaining why the addition of additives inhibits the oscillatory dependence of the capacitance with the pore size.[26] The weak variation of the integral capacitance with the pore size can be attributed to the insensitivity of the EDL structure when it consists of a mixture of counterions and additive molecules. In the smaller pores, the depletion of coions contributes a larger net charge at the surface and disturbs the layer-by-layer ionic

distributions. As a result, the oscillatory dependence of the integral capacitance on the pore size diminishes.

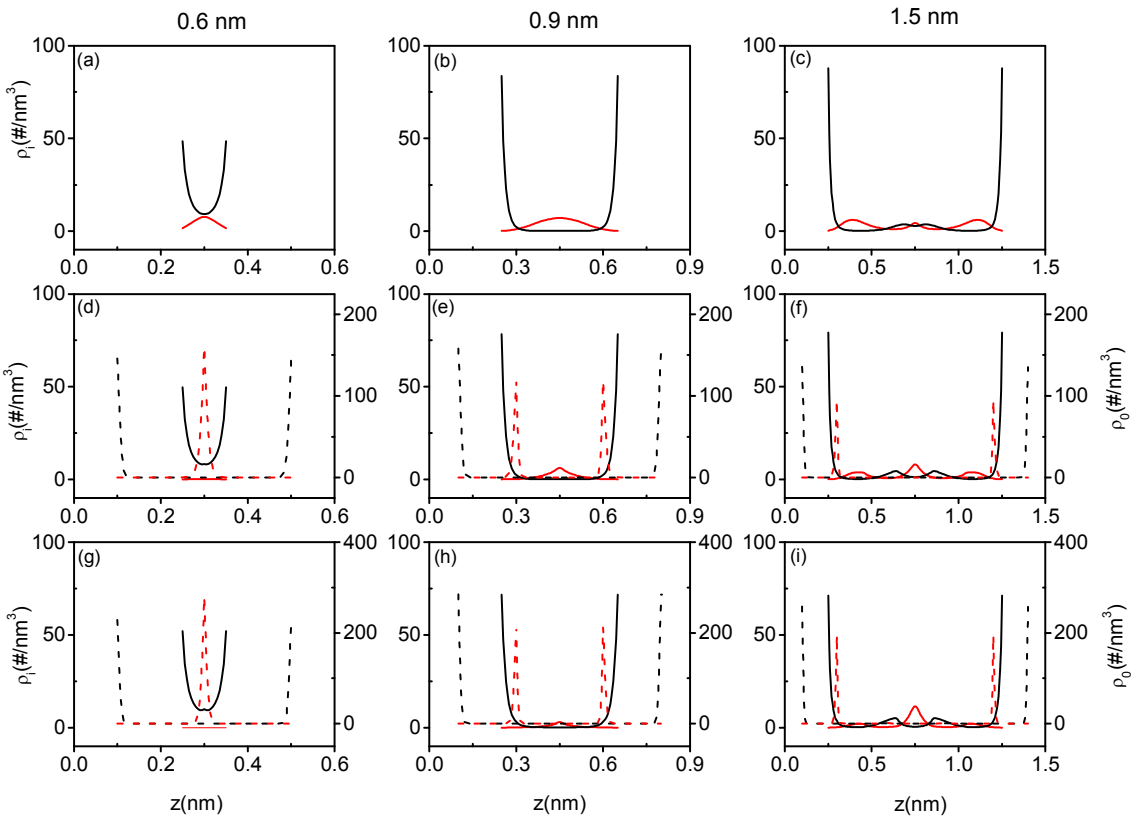

Figure 5 The density profiles of anions (black solid lines), cations (red solid lines), the negative segments (black dashed lines) and the positive segments (red dashed lines) of the additive molecules across slit pores of three representative widths. In all cases, the surface potential is fixed at +1.5 V; the three rows correspond to pure ionic liquid (~3.8M) and ionic liquids with additive molecules of 3.0 D and 3.5 D in dipole moment, respectively.

IV. Conclusions

We have studied how polar additives may influence the layering structure and the integral capacitance of ionic-liquid-based supercapacitors with porous electrodes. Due to the electrostatic attraction from the ionic species and the electrode, the additive molecules of low molecular weight and strong polarity can accumulate in the nanopores even at a very low bulk density. The competitive adsorption of counterion and additive molecules alters the EDL structure and the net

charge at the electrode surface, leading to a drastic increase of the integral capacitance. Importantly, the additive may inhibit the pore size effect thereby enabling broader usage of low-cost amorphous electrodes without scarifying the performance. The theoretical results suggesting that the energy density of supercapacitors can be significantly improved by introducing highly polar additive should be testable with experiments or more elaborate theoretical investigations such as atomistic simulations.

ACKNOWLEDGMENTS

This research is sponsored by the Fluid Interface Reactions, Structures, and Transport (FIRST) Center, an Energy Frontier Research Center funded by the U.S. Department of Energy (DOE), Office of Science, Office of Basic Energy Sciences. This research used resources of the National Energy Research Scientific Computing Center, a DOE Office of Science User Facility supported by the Office of Science of the U.S. Department of Energy under Contract No. DE-AC02-05CH11231.

References:

(1) Salanne, M.; Rotenberg, B.; Naoi, K.; Kaneko, K.; Taberna, P.-L.; Grey, C.; Dunn, B.; Simon, P. *Nature Energy* **2016**, *1*, 16070.
(2) Simon, P.; Gogotsi, Y. *Accounts of Chemical Research* **2012**, *46*, 1094.
(3) Vatamanu, J.; Bedrov, D. *J Phys Chem Lett* **2015**, *6*, 3594.
(4) Kondrat, S.; Wu, P.; Qiao, R.; Kornyshev, A. A. *Nature materials* **2014**, *13*, 387.
(5) Van Aken, K. L.; Beidaghi, M.; Gogotsi, Y. *Angewandte Chemie International Edition* **2015**, *54*, 4806.
(6) Zhong, C.; Deng, Y.; Hu, W.; Qiao, J.; Zhang, L.; Zhang, J. *Chemical Society reviews* **2015**, *44*, 7484.
(7) Lian, C.; Liu, K.; Van Aken, K.; Gogotsi, Y.; Wesolowski, D.; Liu, H.; Jiang, D.; Wu, J. *ACS Energy Letters* **2016**, *1*, 21.
(8) Alam, M. T.; Islam, M. M.; Okajima, T.; Ohsaka, T. *The Journal of Physical Chemistry C* **2007**, *111*, 18326.
(9) Kornyshev, A. A. *The Journal of Physical Chemistry B* **2007**, *111*, 5545.
(10) Feng, G.; Zhang, J.; Qiao, R. *The Journal of Physical Chemistry C* **2009**, *113*, 4549.
(11) Uysal, A.; Zhou, H.; Feng, G.; Lee, S. S.; Li, S.; Cummings, P. T.; Fulvio, P. F.; Dai, S.; McDonough, J. K.; Gogotsi, Y. *Journal of Physics: Condensed Matter* **2014**, *27*, 032101.
(12) Wang, G.; Zhang, L.; Zhang, J. *Chemical Society Reviews* **2012**, *41*, 797.

(13) Simon, P.; Gogotsi, Y. *Nature Materials* **2008**, *7*, 845.
(14) Frackowiak, E.; Abbas, Q.; Beguin, F. *J Energy Chem* **2013**, *22*, 226.
(15) Zhong, C.; Deng, Y. D.; Hu, W. B.; Qiao, J. L.; Zhang, L.; Zhang, J. J. *Chemical Society Reviews* **2015**, *44*, 7484.
(16) Balducci, A.; Dugas, R.; Taberna, P.-L.; Simon, P.; Plee, D.; Mastragostino, M.; Passerini, S. *Journal of Power Sources* **2007**, *165*, 922.
(17) Galiński, M.; Lewandowski, A.; Stępniak, I. *Electrochimica Acta* **2006**, *51*, 5567.
(18) Armand, M.; Endres, F.; MacFarlane, D. R.; Ohno, H.; Scrosati, B. *Nature materials* **2009**, *8*, 621.
(19) Lian, C.; Jiang, D. E.; Liu, H. L.; Wu, J. Z. *J Phys Chem C* **2016**, *120*, 8704.
(20) Largeot, C.; Portet, C.; Chmiola, J.; Taberna, P. L.; Gogotsi, Y.; Simon, P. *J. Am. Chem. Soc.* **2008**, *130*, 2730.
(21) Huang, J. S.; Sumpter, B. G.; Meunier, V. *Angew. Chem.-Int. Edit.* **2008**, *47*, 520.
(22) Huang, J. S.; Sumpter, B. G.; Meunier, V. *Chem.-Eur. J.* **2008**, *14*, 6614.
(23) Centeno, T. A.; Sereda, O.; Stoeckli, F. *Phys. Chem. Chem. Phys.* **2011**, *13*, 12403.
(24) Shim, Y.; Kim, H. J. *Acs Nano* **2010**, *4*, 2345.
(25) Kondrat, S.; Georgi, N.; Fedorov, M. V.; Kornyshev, A. A. *Phys. Chem. Chem. Phys.* **2011**, *13*, 11359.
(26) Jiang, D.-e.; Jin, Z.; Henderson, D.; Wu, J. *The Journal of Physical Chemistry Letters* **2012**, *3*, 1727.
(27) Jäckela, N.; Rodnera, M. ; Schreibera, A.; Jeongwooka, J.; Zeigera, M.; Aslana, M. ; Weingartha, D.; Presser, V. *Journal of Power Sources* **2006**, *doi:10.1016/j.jpowsour.2016.03.015*.
(28) Jiang, D.-e.; Wu, J. *The Journal of Physical Chemistry Letters* **2013**, *4*, 1260.
(29) Feng, G.; Cummings, P. T. *The Journal of Physical Chemistry Letters* **2011**, *2*, 2859.
(30) Jiang, D.-e.; Jin, Z.; Wu, J. *Nano Letters* **2011**, *11*, 5373.
(31) Feng, G.; Huang, J. S.; Sumpter, B. G.; Meunier, V.; Qiao, R. *Phys. Chem. Chem. Phys.* **2011**, *13*, 14723.
(32) Shim, Y.; Jung, Y.; Kim, H. J. *J Phys Chem C* **2011**, *115*, 23574.
(33) Bozym, D. J.; Uralcan, B.; Limmer, D. T.; Pope, M. A.; Szamreta, N. J.; Debenedetti, P. G.; Aksay, I. A. *J Phys Chem Lett* **2015**, *6*, 2644.
(34) Uralcan, B.; Aksay, I. A.; Debenedetti, P. G.; Limmer, D. T. *J Phys Chem Lett* **2016**, *7*, 2333.
(35) Jiang, D.-E.; Wu, J. *Nanoscale* **2014**, *6*, 5545.
(36) Li, Z.; Wu, J. *The Journal of Physical Chemistry B* **2006**, *110*, 7473.
(37) Wu, J., Jiang, T., Jiang, D.-e., Jin, Z. and Henderson, D., *Soft Matter* **2011**, *7*, 11222.
(38) Li, Z.; Wu, J. *Physical Review Letters* **2006**, *96*, 048302.
(39) Jiang, J.; Blum, L.; Bernard, O.; Prausnitz, J. M. *Molecular Physics* **2001**, *99*, 1121.
(40) Jiang, J.; Liu, H.; Hu, Y.; Prausnitz, J. M. *The Journal of chemical physics* **1998**, *108*, 780.
(41) Roth, R.; Evans, R.; Lang, A.; Kahl, G. *Journal of Physics: Condensed Matter* **2002**, *14*, 12063.
(42) Yu, Y.-X.; Wu, J. *The Journal of Chemical Physics* **2002**, *117*, 10156.
(43) Griffin, J. M.; Forse, A. C.; Wang, H.; Trease, N. M.; Taberna, P.-L.; Simon, P.; Grey, C. P. *Faraday Discussions* **2014**, *176*, 49.

(44) Forse, A. C.; Merlet, C.; Griffin, J. M.; Grey, C. P. *Journal of the American Chemical Society* **2016**, *138*, 5731.
(45) Mehio, N.; Dai, S.; Wu, J.; Jiang, D. e. *Nanocarbons for Advanced Energy Storage, Volume 1* **2015**, 361.